geosciences

MDPI

Article

Quantifying Aperiodic Cliff Top and Cliff Face Retreat Rates for an Eroding Drumlin on Ireland's Atlantic Coast Using Structure-from-Motion

Gregor M. Rink [1,2,*], Eugene J. Farrell [3] and Gordon R. M. Bromley [1,2]

[1] Palaeoenvironmental Research Unit, Geography, University of Galway, H91 TK33 Galway, Ireland
[2] SFI Research Centre in Applied Geosciences (iCRAG), O'Brien Centre for Science (East), University College Dublin, Belfield, D04 C1P1 Dublin, Ireland
[3] Geography and Ryan Institute, University of Galway, H91 TK33 Galway, Ireland; eugene.farrell@universityofgalway.ie
* Correspondence: g.rink1@universityofgalway.ie

Abstract: Globally, the rapid retreat of coastal cliffs poses a profound risk to property, transport infrastructure, and public safety. To quantify and compare cliff top and cliff face retreat and identify erosion processes, this study combines historical (1842–2000) maps and orthophotos with contemporary UAV surveys (2019–2023) to quantify cliff top and cliff face retreat along a 240 m wide coastal drumlin in Galway Bay, Ireland. Retreat rates for the cliff top and cliff face were calculated using 2D mapping and 3D modelling, respectively. Critically, the choice of method has a significant impact on calculated rates of cliff top retreat, with output from the 2D mapping approach ($0.14 +/- 0.02$ m yr^{-1}) being double that of the 3D modelling approach ($0.08 +/- 0.02$ m year^{-1}). The aperiodic development of a talus cone, which temporarily protects the cliff from storm waves, also influences estimates of cliff retreat. The repeat cycles of talus slope formation and removal in this high wave energy environment suggest that the drumlin scarp transitions between a periodically transport-limited and supply-limited system over short- and long-time periods, respectively, on the continuum of cliff types. These results warrant further research to identify and quantify the rates, patterns, drivers (marine and subaerial processes), and timing of cliff retreat in response to climate change.

Keywords: soft rock cliff erosion; coastal erosion; structure-from-motion; cliff top line detection

Citation: Rink, G.M.; Farrell, E.J.; Bromley, G.R.M. Quantifying Aperiodic Cliff Top and Cliff Face Retreat Rates for an Eroding Drumlin on Ireland's Atlantic Coast Using Structure-from-Motion. *Geosciences* **2024**, *14*, 165. https://doi.org/10.3390/geosciences14060165

Academic Editors: Fabrizio Antonioli and Jesus Martinez-Frias

Received: 8 March 2024
Revised: 13 May 2024
Accepted: 22 May 2024
Published: 12 June 2024

1. Introduction

In Ireland, the geomorphic impacts of Late Pleistocene glaciation are particularly evident along the west coast, where the convergence of ice flow and a ready sediment supply has resulted in the widespread formation of coastal drumlins [1]. In those locations where drumlins intersect the modern intertidal zone, chronic coastal erosion is prevalent, resulting in the undercutting of cliffs, slope failure, and the subsequent release of large volumes of sediment into local littoral cells. Instances of this phenomenon have been documented in Clew Bay [2], Strangford Lough [3], and Galway Bay [4]. As waves and tides remove the fine-grained glaciogenic sediments, coarse clastic material is often left behind within the intertidal zone, where it forms a residual lag that serves as a protective barrier against erosion [1]. Depending on their size, exposure to storm waves and regional rates of sea level rise, actively eroding drumlins can potentially supply new sediment for marine dispersal for the next 500 to 2000 years [3]. Therefore, an improved understanding of these sediment storage and transfer systems is important for establishing the short- and long-term drivers shaping Ireland's contemporary coastline. Further, quantifying erosion rates of glacial cliffs provides valuable information for local decision-makers tasked with managing the growing risk of coastal geohazards due to coastal erosion, particularly if these are linked to anthropogenic climate change [5].

Cliffs form approximately 80% of the global coastline and exhibit highly variable rates of erosion and retreat [6–8]. It is estimated that approximately 56% of Ireland's 5400 km long coast is dominated by rocky shorelines, of which ~1288 km is categorised as cliffs; an additional 170 km comprises composite cliffs featuring a mix of hard and soft materials [9]. Cliff retreat rates depend on local parameters such as lithology and slope of the cliff, local climate and tidal range, wave dynamics, sea level trends, and the intertidal and marine environments adjacent to the cliff [7,10]. Previous studies have applied different research techniques to analyse cliff changes and erosion rates at numerous sites around the world. Among the most commonly reported methods are structure-from-motion (SfM) (e.g., [11–13]), analysis of historical maps and aerial photographs (e.g., [13–15]) and terrestrial light detection and ranging (LiDAR) [16–18]. SfM is a photogrammetric approach that is now applied widely in geoscience disciplines, including geomorphology (e.g., [12,19,20]) and glaciology (e.g., [21,22]), to detect landform changes. Exploiting the recent refinement of uncrewed aerial vehicle (UAV) technology, large tracts of even the most inaccessible coastlines can now be mapped accurately, safely, and at relatively low costs [11,12,23]. Digital surface models (DSM) and three-dimensional points clouds (PC) of coastal cliffs and adjacent rock platforms can be computed with very high spatial and temporal resolution when georeferenced using ground control points (GCPs). Together, these methods can provide highly accurate baseline data to detect changes in volume and cliff retreat rates [11,24]. Augmenting these observational data, secondary sources derived from historical maps and satellite imagery can provide valuable additional information and invaluable long-term context for the geomorphological change detection analyses. Spanning timescales of decades and centuries, these secondary data are especially important for investigations of coastal landform responses to climate change and anthropogenic pressures [15,25,26], particularly where historical mapping covers several centuries [14,27,28]. In Ireland, the first accurate large-scale maps (six inches represents one mile on the ground) were published during the 19th century by the Ordnance Service Ireland (OSI) [28].

Depending on the data available, investigations into cliff retreat rates generally rely on one of three key methods. The first method estimates cliff retreat directly from changes in cliff top position, either from historical maps or orthophotos (e.g., [13,14,26,27]), while the second method employs erosional pins deployed near the base of the cliff to monitor changes in cliff face position (e.g., [3,29]). More recently, the development of UAV and LiDAR technologies has provided a third method by providing high-resolution 3D modelling of cliff retreat from remotely sensed data [11,13,19]. To reduce the dependency on the mentioned technologies and to increase the size and temporal resolution of datasets, approaches of including crowd-sourced data in SfM analysis were tested by [30,31]. Recognising that methodology is largely dictated by data availability, prior research confirms that the choice of cliff top or cliff face estimates has the potential to influence results. For example, Refs. [19,32] both reported measurable differences between cliff top-derived and cliff face-derived retreat rates in studies of the same cliff. Nonetheless, the processes driving changes in the cliff face and cliff top configuration are intrinsically coupled via an erosion–deposition cycle [7,10,32]. Cliff face erosion undercuts the cliff, resulting in cliff top failure and the formation of a talus cone at the cliff base; this cone protects the cliff face from further erosion until it is removed by wave action, whereupon undercutting resumes [10,16,17,32–34]. Refs. [35,36] both demonstrated that erosion of soft rock cliffs can vary widely over time and that high-energy storms with extended wave run-up can dramatically increase erosion rates on short event timescales.

Previous studies of coastal cliffs in Ireland [3,35–37] and the UK [11,19,38–41] have reported considerable variability in cliff retreat rates (Table 1). Hard rock cliffs composed of sandstones, limestones, basalts, and granites often have very low annual retreat rates (0.001–0.1 m) [19,37,38], whereas cliffs comprising softer rock material, such as chalk and glacial till, exhibit much higher rates in the range of decimetres per year [3,34,39,40]. In Ireland, drumlins are prominent features on the landscape and represent evidence of the passage of glacier ice during the Quaternary. In west coast locations such as Galway

Bay and Clew Bay (Co. Mayo), drumlins are a quintessential feature of the otherwise rocky coastlines. In almost every case, coastal drumlins in the west of Ireland exhibit severely eroded cliff faces, exposing the landform interior of till and glaciofluvial sediments [3,4].

In this study, we measured changes along a 250 m long escarpment that forms the southern margin of a drumlin at Silverstrand, Galway Bay, on Ireland's west coast. Being surveyed regularly since the 19th century by the OSI [28] and the University of Galway [41], this study site allows the combination of historical 2D mapping (1842), orthophotography (1995, 2000), and UAV surveys (2019, 2022, and 2023). For our analyses, we used a coupled 2D morphometric–3D modelling approach to quantify changes in the cliff top and cliff face over timescales ranging from months to a century.

Table 1. Summary of previous studies estimating coastal cliff retreats in Ireland and Great Britain.

Study	Region	Cliff Lithology	Age	Study Period	Number of Cliffs	Total Studied Cliff Length	Methods	Retreat Rate (m/year)
[3]	Strangford Lough, UK	Till	Holocene	3	16		Historical maps, aerial photographs	0.01–0.16
[34]	Portballintrae, UK	Till	Holocene	156	5		Historical maps, aerial photographs	0.00–0.52
[37]	N Yorkshire, UK	Sandstone, mudstone	Jurassic	3	2	20.459 km	Historical maps, aerial photographs	0.02–0.10
[38]	Bideford, UK	Sandstone, mudstone	Carboniferous		1		Historical maps, aerial photographs	0.01–0.03
[39]	St. Margarets, UK	Chalk	Cretaceous	122	1	~5.5 km	Historical maps, aerial photographs	0.07 +/− 0.043
[40]	E Sussex, UK	Chalk	Cretaceous	128	5	23 km	Historical maps, aerial photographs	0.27–0.41

2. Study Site

2.1. Physiographic Setting

Our study site is the Knocknagoneen drumlin, located immediately west of Galway City on the northern shore of Galway Bay (53°15′1.00″ N, 9°7′23.00″ W) (Figure 1). The Knocknagoneen drumlin is the most westerly of three neighbouring drumlins (Figure 1) [4,42] and contributes circa 41–64% of its eroded material to the adjacent fringing barrier (stony bank) and an ecologically important inner saltmarsh estuarine ecosystem (Rusheen Bay) that is currently protected by multiple European environmental designations (SAC 0268, SPA 4031) [41]. Local sediment dynamics are dictated by marine forces acting upon the three drumlins (Figures 1 and 2). The drumlin's vertical cliff face is as much as 17 m high and approximately 240 m in length (Figure 3). Fronting the cliff is a subhorizontal platform of glacial boulders set into clay-rich till, analogous to a Type-A shore platform on the Sunamura scheme [32]. Satellite imagery provides strong evidence of the platform's size and shape (extending 235 m from the cliff), which together demark the original extent of the drumlin prior to erosion (Figure 1). Eroded drumlin material can form a temporary talus slope at the cliff's base (Figures 3 and 4). Approximately 750 m north-east of Knocknagoneen, the Knocknacarragh drumlin exhibits a similar size and form to its neighbour: the 260 m long cliff is ~15 m high at its mid-point (Figure 2). In contrast, the smallest of the three drumlins, Illaunafamona, exhibits a more limited seaward cliff (<20 m long, ~10 m high) but highly eroded lateral margins (Figure 2).

Being located circa 33 km east of the Aran Islands in the inner bay, the Silverstrand drumlins are relatively protected from the full erosive power of the North Atlanticirca Nevertheless, this site experiences a strongly oceanic climate, with year-round wind and high precipitation [43,44], winter storm surges and semidiurnal tides of ~2–5 m [45–47]. From our observation, during spring tides, the high tide water line reaches the cliff base,

while during low tide, the shore platform is almost fully exposed (beach width around 250 m). In interior Galway Bay, waves generally travel from southwest to north-east and exhibit significant wave heights of 2.5–3.0 m [46–48]; significant wave height increases considerably during storm events [46,47] and the winter season [48]. According to the classification scheme for soft coastal cliffs, the expected potential hazard level for the site is 'high to very high' [49].

The average monthly precipitation recorded at Inis Mór, the most north-western of the Aran Islands located at the mouth of Galway Bay circa 40 km from the study site (Figure 1), is 107 mm, and the number of rain days (0.2 mm or more) per month is 21 for the period January 2018–October 2023 (70 months).

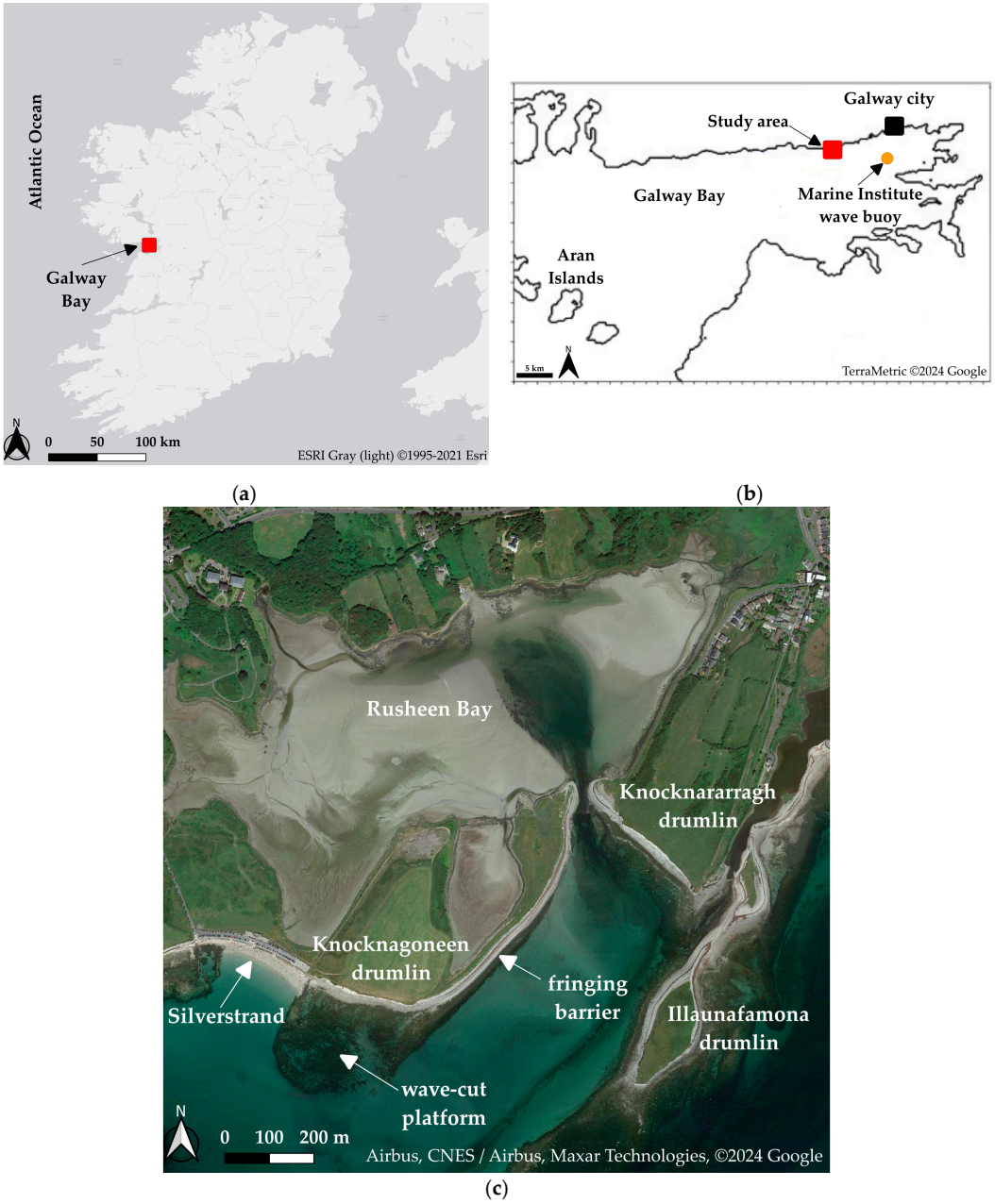

Figure 1. (**a**) Location of Galway Bay on west coast of Ireland. (**b**) Location of the Knocknagoneen drumlin (study area), Galway Bay. (**c**) Satellite image of the study area showing the position of the Knocknagoneen drumlin and adjacent features (Silverstrand, wavecut platform, fringing barrier, and Rusheen Bay). Basemaps are sourced from (**a**), ESRI Gray (light) ©1995cal –2021 Esri [50], (**b**) TerraMetric ©2024 Google, and (**c**) Airbus, CNES/Airbus, Maxar Technologies, ©2024 Google [51].

Figure 2. South-east facing oblique aerial photograph of the study area, showing the downward sloping western cliff face of the Knocknagoneen drumlin (left background) separated from the Knocknacarragh drumlin (right background) by a fringing barrier and tidal inlet feeding Rusheen Bay (middle background). The Illaunafamona drumlin is in the foreground.

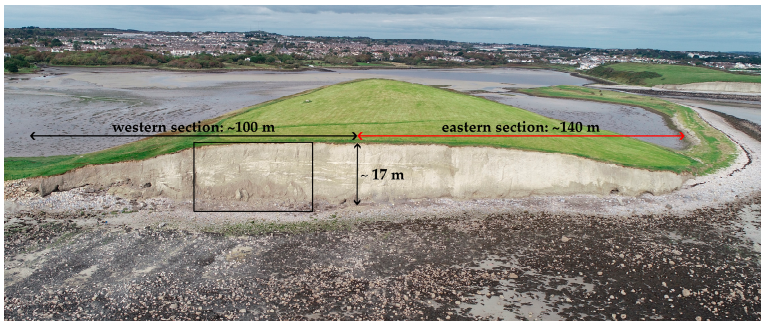

(**a**)

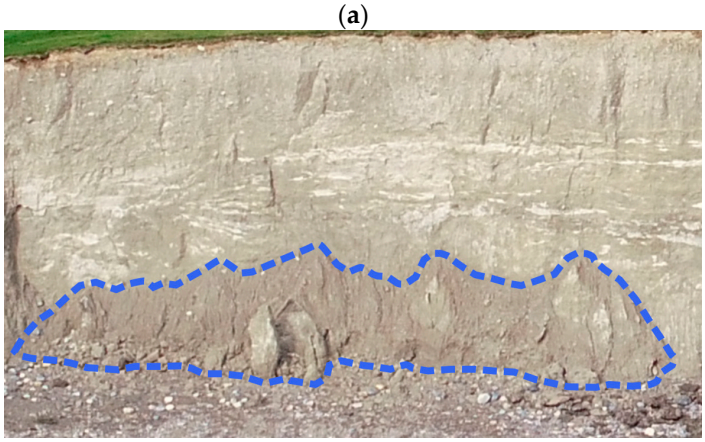

(**b**)

Figure 3. (**a**) South-east facing oblique aerial photograph of the exposed cliff face of the Knocknagoneen drumlin. The black rectangle denotes the area shown in panel b. (**b**) Close-up photograph highlighting the talus slope (**- -**) at the cliff base in (**a**) on 2 October 2019.

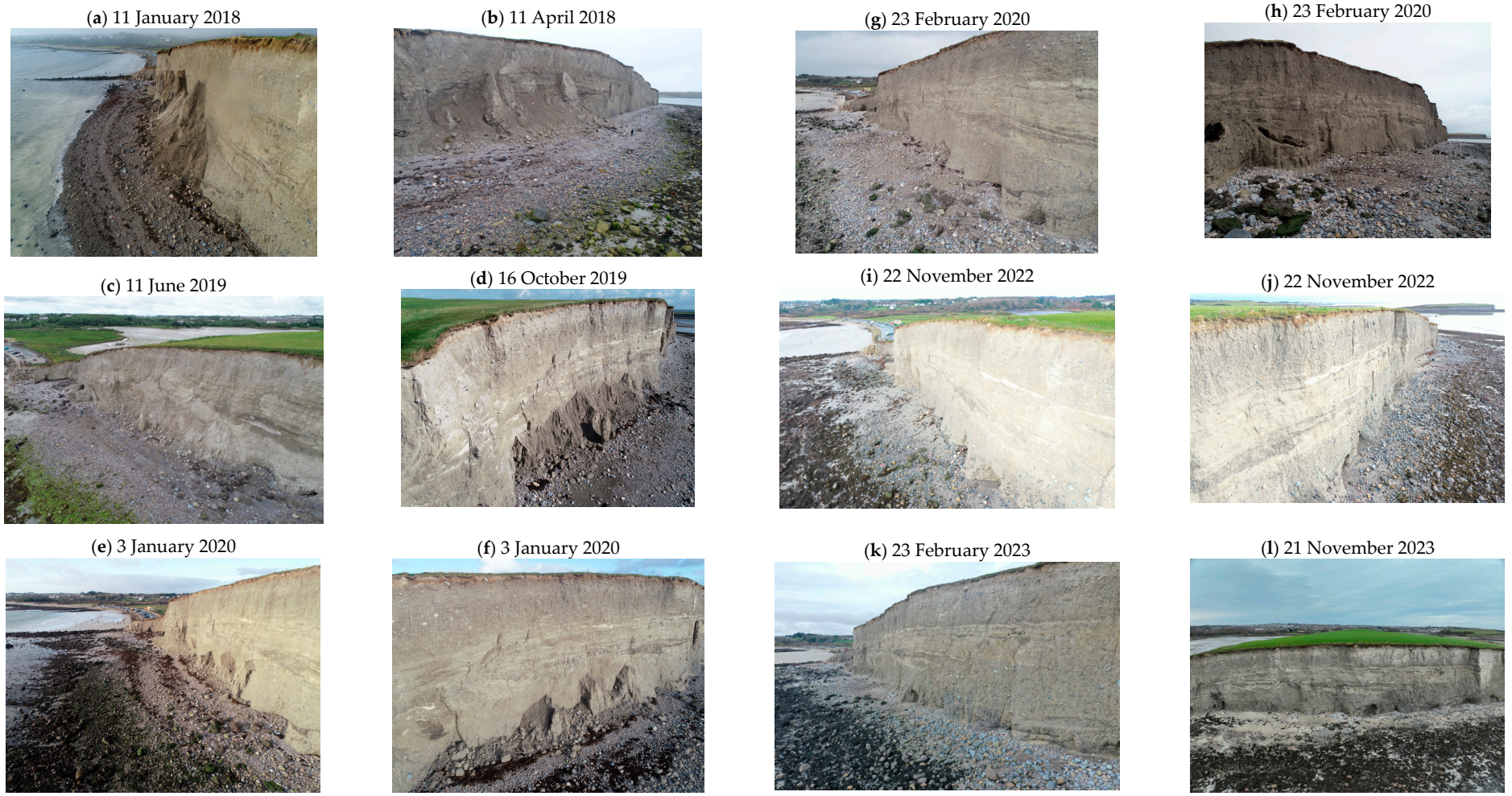

Figure 4. Oblique aerial photographs of the Knocknagoneen drumlin from January 2018 and November 2023. Although the cliff was not surveyed during the 2018–2019 winter season, the first survey of 2019 reveals evidence for the former extent of a major talus cone that developed during that interval. The talus slope was removed in the 2019–2020 winter season. Note the figure standing near the base of the cliff in panel (**b**) for scale. The talus slope was not present between spring 2020 and winter 2023.

2.2. Geological History

The Knocknagoneen drumlin is a product of the Quaternary ice ages, during which Ireland's landscape was profoundly shaped by the passage of glacier ice [4]. As a composite drumlin, Knocknagoneen comprises sediments derived from multiple pulses of glaciation. In their sedimentological study of the cliff face, Ref. [4] identified four general lithofacies that become gradually coarser-grained with height: muddy diamict at the base is overlain by a pebble-rich diamict, which is overlain in turn by a unit of finer-grained sediments capped with a boulder-rich till. Our own investigations of the drumlin face reveal varved sediments and coarse alluvial material within the basal few metres, indicative of ice-free deposition prior to subsequent glacial overriding. Granite and limestone clasts are common throughout the exposure (Figure 5). Together, the drumlin's sedimentology is reinterpreted as reflecting a mixture of subaquatic and subglacial deposition, which is common at the margins of marine-terminating ice sheets [4]. Previous studies examining ice flow directions using striae indicate that the ice flow direction was south to southwest [52,53], which is reflected in the S-SW orientation of the drumlin [54,55].

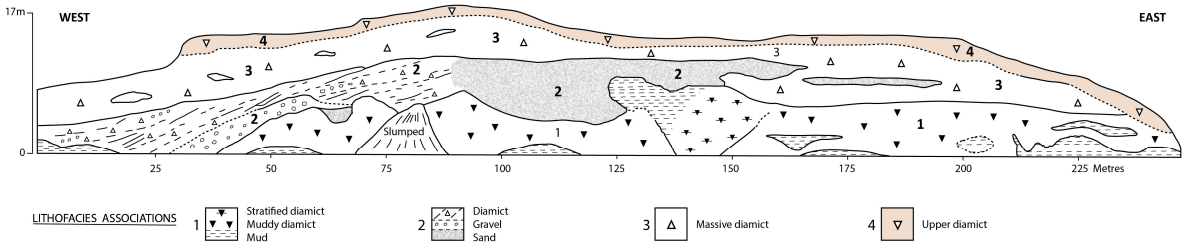

Figure 5. Cross section of the Knocknagoneen drumlin, modified from [4], depicting the four different lithofacies described in that study.

Following the deglaciation of Galway Bay at approximately 17 ka [56], our study area remained above sea level for several millennia before marine incursion during the middle Holocene. At Spiddal beach, ~13 km west of Silverstrand, in situ stumps of mature oak, pine, and birch trees are exposed periodically by storm erosion and afford maximum-limiting radiocarbon ages of 7.4–4.8 cal ka BP for the onset of marine conditions [57,58]. This range aligns with palaeohydrological reconstructions from Loch Mór, Inis Oírr, the south-easternmost of the Aran Islands (Figure 1), which suggests that the sea level adjacent to Galway Bay attained its modern configuration of approximately 5.1 ka [59]. At this point, we posit that marine forces began to erode the Knocknagoneen drumlin [4], manifesting in the formation of the distinct cliff morphologies seen today. While Knocknagoneen's original morphology is no longer visible, the intertidal shore platform described above confirms the drumlin's original footprint and provides a longer-term context for the erosion rates discussed below.

3. Materials and Methods

For this study, we used historical maps, orthophotos, and recent UAV surveys to investigate changes in cliff top and cliff face position at Knocknagoneen (Table 2). The cliff top changes were analysed using the Shoreline Analysis System (DSAS) Version 5.0 [60,61] in ArcMap 10.4, while cliff face changes were detected using a multiscale model-to-model cloud comparison (M3C2) in CloudCompare, v2.13 alpha [62,63]. A detailed overview of the workflows is given in Figure 6.

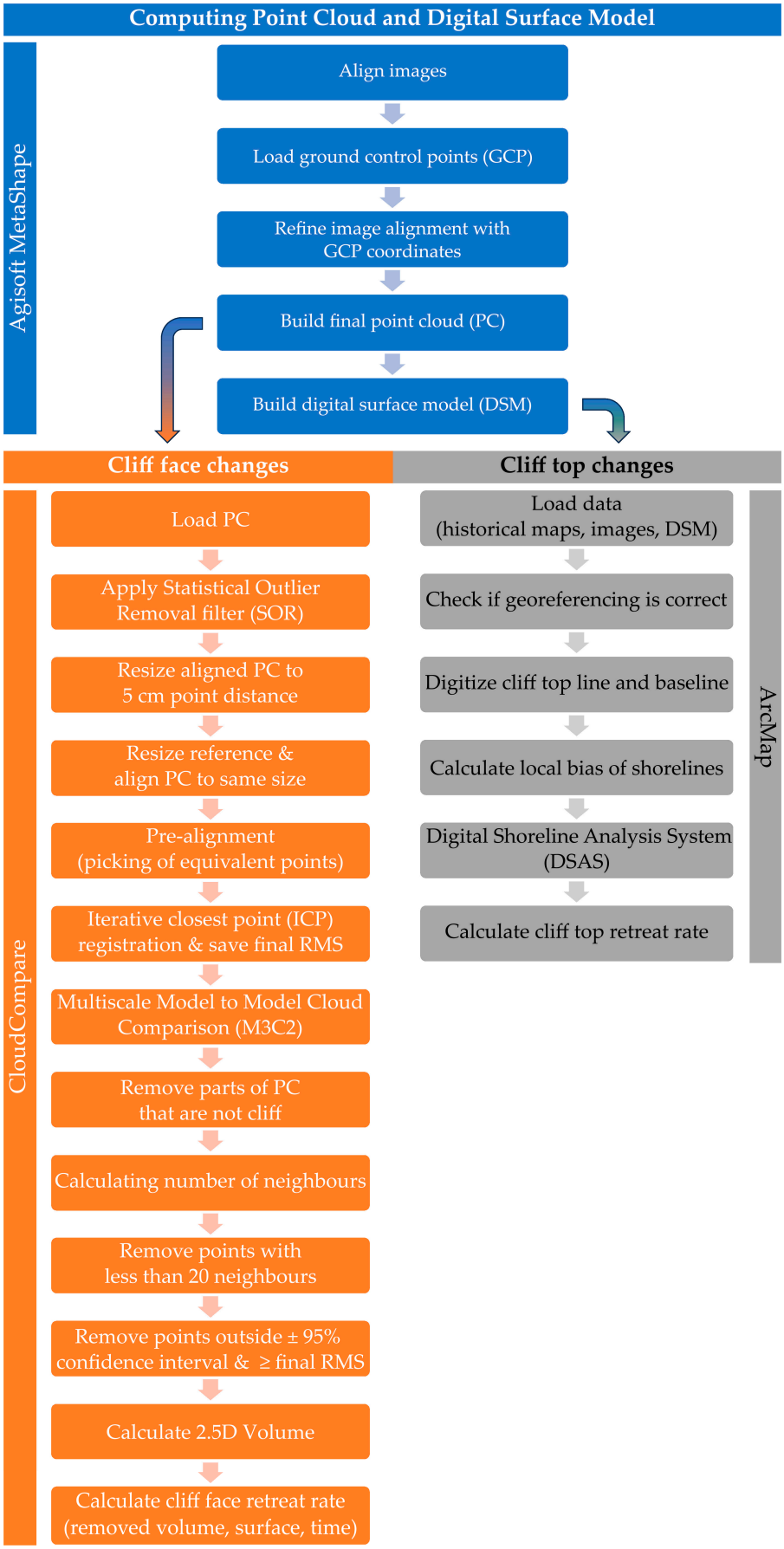

Figure 6. Step-by-step workflow to compute PCs and DSMs from UAV imagery.

Table 2. Overview of the primary and secondary data sources used in this study. Data were purchased from the Ordnance Survey Ireland (OSI) and derived from their own surveys using uncrewed aerial vehicles (UAV).

Data Source	Date	Feature	UAV Model	Images Collected	GCPs
OSI 6" map	1842	Cliff top			
OSI orthophoto	1995	Cliff top			
OSI orthophoto	2000	Cliff top			
UAV	11 June 2019	Cliff face	DJI Phantom 4 Pro	118	6
UAV	2 October 2019	Cliff face	DJI Phantom 4 Pro	257	9
UAV	5 October 2019	Both	DJI Phantom 4 Pro	185	5
UAV	22 November 2022	Cliff face	DJI Mavic 2 Pro	321	9
UAV	21 September 2023	Both	DJI Mavic 3M	348	5
UAV	21 November 2023	Cliff face	DJI Mavic 3M	513	9

3.1. Structure from Motion

3.1.1. SfM Data Acquisition

Following similar workflows to those reported in [11–13] and elsewhere, we used brightly coloured spray paint to create GCPs (~0.40 m long X-shaped markings) both in the intertidal zone at the cliff base and atop the drumlin near the cliff edge. The GCP coordinates were collected using accurate (0.02–0.03 m) Trimble R8 PPK and R10 RTK Global Navigation and Satellite Systems (GNSS). We used a UAV to collect near-vertical (80°), overlapping (75–80%) images of the entire cliff surface with a flight altitude of 55–65 m; the average ground sampling distance resolution was between 0.01 m and 0.03 m. Additionally, we captured horizontal images of the cliff face. These images, in conjunction with the GCPs, enabled us to build accurate PCs and DSMs within the workflow outlined in Figure 6. In all, we conducted six field surveys at low tide: 11 June 2019, 2 October 2019, 5 October 2019, 22 November 2022, 21 September 2023, and 21 November 2023 (Table 2).

3.1.2. SfM Data Processing

Computation of PCs and DSMs

We used Agisoft Metashape (Version 1.5.5 9097) to generate PCs and DSMs in line with the workflow described by [64]. For most of the surveys, the angle of 80° ensured good coverage of both the cliff top and cliff surface, thereby precluding the need for additional horizontal images. However, for the 22 November 2022 survey, we incorporated horizontal imagery to improve the overall quality of the PC. First, we detected the respective GCP configuration deployed during each field survey and assigned them coordinates using the Irish Transverse Mercator (IRENET95, EPSG: 2157 coordinate system). For the first four surveys, we applied default settings for image alignment (key point limit = 40,000 and tie point limit = 10,000) and set accuracy to "highest". To capitalise on the improved camera resolution of the last two surveys, we set the key point and tie point limits to 60,000 and 0, respectively [64], with accuracy remaining at "highest". The quality of the camera alignments was assessed prior to generating high-resolution PCs. Once these had been generated, we used the PCs to calculate DSMs. Specifically, the 5 October 2019 and 21 September 2023 DSMs were used to measure changes in the position of the cliff top. After GCP-based georeferencing, the final RMS errors were 0.013 m for the 5 October 2019 survey (0.012 and 0.003 m in the horizontal and vertical directions, respectively) and 0.026 m for the 21 September 2023 survey (0.021 m and 0.014 m in the horizontal and vertical directions, respectively). All UAV surveys were implemented to measure cliff face retreat using PC registration and the iterative closest-point algorithm.

For PC alignment and change detection analysis, we used CloudCompare v2.13. alpha [63] following the protocols described by [11,13,62,65]. Since each PC is aligned to the same reference PC, specific GCPs were not needed for registration. We separated PCs into two sections, representing the western and eastern portions of the cliff, to reduce the

final registration errors [13,62]. Prior to alignment, each PC was filtered using a statistical outlier removal filter that applies nSigma = 1 and 6-point mean distance estimates [13]. Owing to its high lateral coverage and high point density, we chose the 11 June 2019 survey to serve as the reference PC for all subsequent surveys (Table 3). This also allows measurements of changes over time linked to a baseline condition [66]. After filtering, the respective PCs for the 2 October 2019, 5 October 2019, 22 November 2022, 21 September 2023, and 21 September 2023 surveys were subsampled to 0.05 m to ensure comparability. The reference PC was not subsampled so as to retain the maximum density of reference point data. To improve PC alignment and minimise analytical error, we conducted quality control in CloudCompare to remove vegetation and any part of the PCs generated from inaccurate computations [62]. Final alignment was made using the Iterative Closest Point Algorithm (ICP) [67] in CloudCompare [63], after which, where necessary, we performed a handpicked rough alignment to predefine corresponding points for the ICP. This approach improved the results of our registration process [67].

Table 3. Overview of reference and comparative survey dates used in the SfM analysis.

Time Period	Reference Survey Date	Comparison Survey Date	Duration between Surveys (Days)
PC-change I	11 June 2019	2 October 2019	1260
PC-change II	11 June 2019	5 October 2019	1563
PC-change III	11 June 2019	22 November 2022	1624
PC-change IV	11 June 2019	21 September 2023	113
PC-change V	11 June 2019	21 November 2023	116

PC Change Detection

We applied the M3C2 algorithm to the five periods listed in Table 3. This algorithm compares two PCs directly, without previous meshing or gridding [62], thereby enabling us to detect specific areas that experienced material loss or gain over time. Since most higher parts of the cliff face are nearly vertical, areas indicating net gain most likely reflect higher registration errors [13]. These areas were excluded from the calculation of erosion and cliff face retreat rates accordingly. Where any apparent change in the position on the cliff face was less than the error of the registration, we assumed that no significant change was detectable within the calculated certainty [62].

Cliff Face Retreat Rate [m yr^{-1}] and Erosion Rate [m^3 yr^{-1}]

Changes in the cliff face configuration were calculated using two different parameters. First, we defined the erosion rate (e_r [m^3 yr^{-1}]) as the amount of volume lost from the cliff face over time. We then defined the cliff face retreat rate (cf_r [m yr^{-1}]) as the horizontal distance the cliff face had receded over the same period. The latter is key to establishing whether there are significant differences between estimates of cliff retreat based on the cliff top position (Section 3.2) or the cliff face, which would have implications for the selection of survey methodologies.

To estimate e_r, we first clipped out the cliff face of the reference PC and that of each subsequent PC, whereafter we used the 2.5D volume algorithm in CloudCompare to calculate respective differences in volume. Specifically, the 2.5D volume is calculated by designating the direction from the grid origin (0/0/0) as the preferred orientation. The best-fit projection direction is Y, reflecting the WNW-ESE orientation of the Knocknagoneen drumlin, which would probably produce an approximately S-N direction of change. We calculated e_r from the volume of material eroded and the time elapsed between surveys [68], while cf_r was calculated as the ratio of the total reference PC surface area and the time elapsed between successive surveys [68].

3.2. Cliff Top Position

3.2.1. Cliff Top Digitization and Error Analysis

We used historical maps and orthophotos provided by OSI (Table 2) and georeferenced to the Irish Transverse Mercator geographic coordinate system for Ireland (IRENET95, EPSG: 2157) [28]. This digitised dataset includes the first coloured 6″ map series of Ireland, which was surveyed in the 1830s and published in 1842, in addition to a black-white orthophoto from 1995 and a colour orthophoto from 2000. Each orthophoto has a reported ground resolution of circa 0.66 m [69]. Since the root mean square errors (RMS) of the georeferenced maps and orthophotos were not provided by OSI, we applied highly conservative estimations for shoreline errors (E_s) based on the suggestions of [14]. These data were supplemented with cliff top lines extracted (manual digitisation in ArcMap) from DSM's generated from our UAV surveys conducted on 5 October 2019 and 21 September 2023 (RMS errors of 0.013 m and 0.026 m, respectively).

3.2.2. Cliff Top Changes

We used DSAS to compute changes in cliff top position over the four periods depicted in Table 4. DSAS is a freely available add-on tool for Esri ArcGis and is applied widely in coastal research [14,15,26,27,70–72]. To detect spatial patterns in cliff top changes and erosion rates, we computed perpendicular shoreline transects every metre along the cliff base. Since the cliff top line is relatively straight, a transect smoothing distance of 500 m was deemed sufficient [60,61]. We adopted the weighted linear regression (WLR) method to calculate rates of cliff top change. This statistical approach is considered reliable because it accounts for the uncertainty field when calculating long-term rates of cliff top change, specifically by designating a higher impact for E_S in the calculation and by adding at least one intermediate cliff top line [61,73]. Based on the E_S of each cliff top line, we calculated weights (w) for each cliff top line and included these in our calculations of shoreline change [61,73]. Higher E_S values signify lower contributions of the corresponding cliff top line to the calculated retreat rate. Finally, we estimated the WLR error by making multiple comparisons of the known distance between the baseline and a cliff top line data point with the predicted value for this distance [61,73].

Table 4. Overview of the analysis via Digital Shoreline Analysis System (DSAS). For data provided by OSI, 01 January was used in lieu of the exact dates of acquisition, these being unavailable.

Time Period	Reference Date	Analysed Date
DSAS I	1842	1 January 2000
DSAS II	1842	5 October 2019
DSAS III	1842	21 September 2023
DSAS IV	1995	21 September 2023

3.3. Storm Event Detection

Wave data were not monitored locally, so the Marine Institute East Atlantic SWAN Wave Model dataset was used to derive wave parameters approximately 4 km offshore of the site at 53°14′15.00″ N, 9°3′45.00″ W in the inner bay (Figure 1b). The model provides a three-hourly significant wave height, wave period, and wave direction. Thresholds for storm detection are site-specific, so the method reported in [74] was used as a guide to identify storm events within the modelled wave conditions. We identified storm events as those during which the peak significant wave height (H_s) exceeded 3 m and storm duration exceeded twelve hours (extending over at least one high tide). The start and end of storms occurred when H_s exceeded or fell below 2 m.

4. Results

4.1. Cliff Face Changes

According to our assessment, the volume of sediment removed from the cliff between 11 June 2019 and 21 November 2023 was 1197 ± 228 m^3 (approximately 3100 tons), a significant proportion (circa 53%) of which reflects the erosion of the talus slope fringing the drumlin's western section (Figure 7c). Accordingly, the western section accounts for 59% of the total sediment loss (711 ± 133 m^3) and the eastern section 41% (486 ± 95 m^3) (Figure 7a). The average rate of cliff face retreat over the same period was −0.34 ± 0.06 m, with the western section experiencing greater recession (−0.46 ± 0.10 m) than the eastern section (−0.22 ± 0.03 m) (Figure 7b).

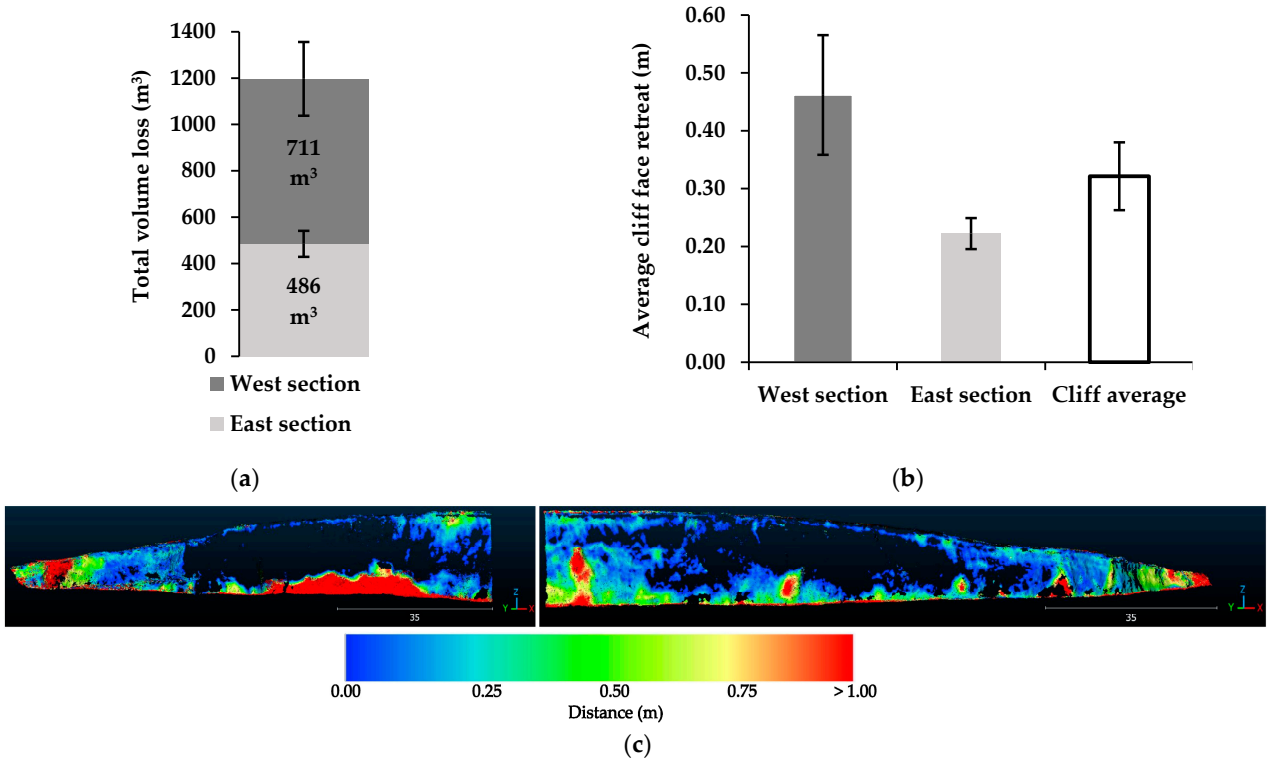

Figure 7. (**a**) Total volume of sediment lost from the cliff face between 11 June 2019 and 21 November 2023. (**b**) Average retreat rate of the cliff face over the same period. (**c**) Erosion of the cliff face along the western (left panel) and eastern (right panel) sections for the same period (note the scale difference between Figures 7c and 8a). The changes were described as distance based on the results from the M3C2 calculations. Black areas within the wall show changes within uncertainty values. Those values include erosion as much as technical accretion. The accretion is assumed to be a result of analysing errors.

We used PC analysis to map the spatial distribution of change along the entire cliff face (Figure 8), which again revealed that estimated cliff face retreat rates (cf_r [m yr^{-1}]) are considerably higher in drumlin's western section than in the eastern section. The most significant changes occurred over the interval from 6 October 2019 to 22 November 2022, reflecting the removal of the talus slope by wave action (see Figure 4). Overall, the higher rates along the western section reflect the removal of the talus slope (circa 5 m), but this spatial variability was reduced after this sediment was removed.

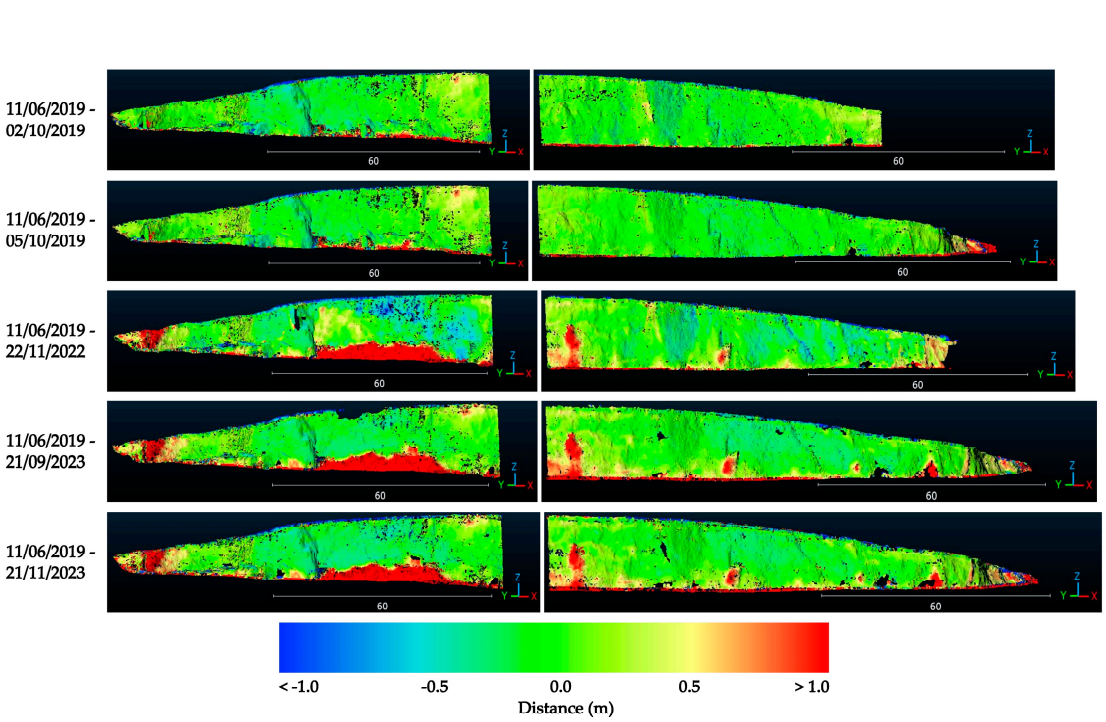

(**a**)

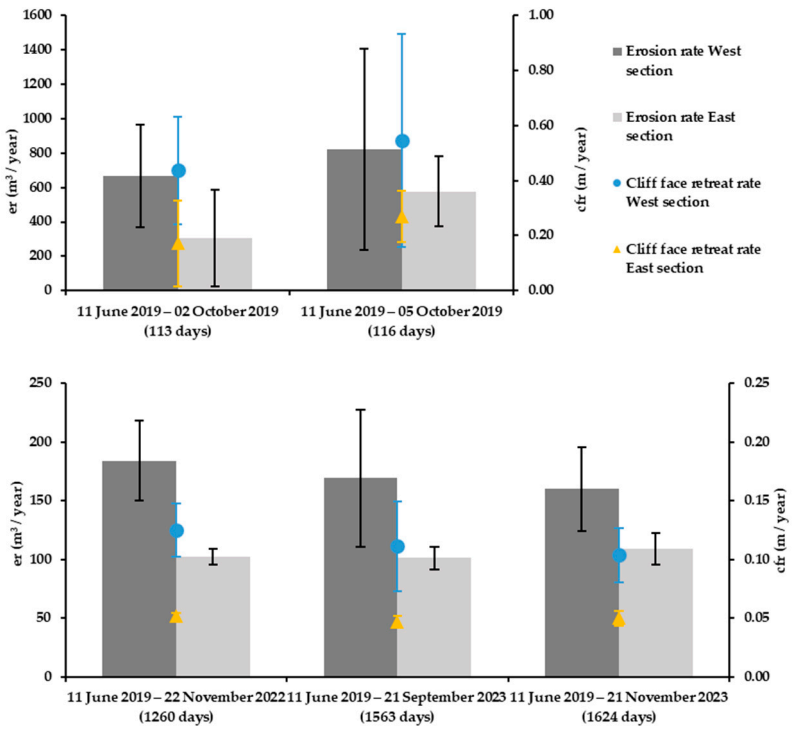

(**b**)

Figure 8. Mapped cliff face changes and calculated rates of erosion and cliff face retreat. (**a**) Cliff face changes in the western (left panels) section and eastern (right panels) sections calculated using PC analysis. Only values outside uncertainty values are shown in colours; values within uncertainty are shown in black. The changes were described as distance based on the results from the M3C2 calculations. Positive values indicate sediment loss, while negative values indicate sediment gain. (**b**) Erosion rates (e_r) and cliff face retreat rates (cf_r) for the western and easter sections. The upper panel depicts the rates of erosion and cliff face retreat between 11 June 2019, 2 October 2019, and 5 October 2019. The lower panel shows the rates for 11 June 2019–22 November 2022, 21 September 2023, and 21 November 2023.

The restricted interval (three days) between our 2 October 2019 and 5 October 2019 surveys coincided with Storm Lorenzo, which passed over Ireland on 3 October 2019 [75]. According to our storm detection analysis, this system failed to satisfy the criteria for being categorised as a storm when it passed Silverstrand. Specifically, the 12 h long event produced average and maximum H_s of 2.43 m and 2.67 m, respectively, which is below the storm detection threshold. Consequently, Storm Lorenzo resulted in minimal change to the drumlin face. Nevertheless, the storm afforded a valuable opportunity to test the applicability and accuracy of the workflow. This analysis confirmed that very little change occurred along the entire cliff face during the event, reinforcing our confidence in the methodology and our subsequent erosion estimates. The highest-magnitude change in the entire study period was observed using the following survey (22 November 2022), by which time the talus slope had been removed entirely (Figure 4).

Using the 11 June 2019 survey as a reference, we observed that cliff face erosion rates are higher for the western section than for the eastern section. Within both sections, the erosion rate is highly consistent, exhibiting values of 160–184 m^3 yr^{-1} and 101–109 m^3 yr^{-1} for the western and eastern sections, respectively. Similarly, retreat rates are also consistent over time, ranging from 0.104 to 0.125 m yr^{-1} for the western section and from 0.047 to 0.052 m yr^{-1} for the eastern section. Averaging the values from both sections of the cliff face affords an estimated cliff erosion face retreat of 134 m^3 yr^{-1} and a cliff face retreat rate of 0.077 m yr^{-1} for the period between 11 June 2019 and 21 November 2023 (1624 days) (Table 5, Figure 8).

Table 5. Cliff face erosion (e_r) and retreat rates (cf_r) observed in 2022 and 2023 relative to the 11 June 2019 baseline survey (see Table 3 for details).

	Western Section		**Eastern Section**	
	e_r [m^3 yr^{-1}]	**cf_r [m yr^{-1}]**	**e_r [m^3 yr^{-1}]**	**cf_r [m yr^{-1}]**
PC-change III	184 +/− 34	0.125 +/− 0.023	102 +/− 6	0.052 +/− 0.003
PC-change IV	169 +/− 59	0.111 +/− 0.038	101 +/− 10	0.047 +/− 0.005
PC-change V	160 +/− 36	0.104 +/− 0.023	109 +/− 13	0.05 +/− 0.006

4.2. Cliff Top Changes

Average cliff top retreat rates (ctr [m yr^{-1}]) are shown in Figure 9 for four different intervals: 1842–2000 (DSAS I), 1842–2019 (DSAS II), 1842–2023 (DSAS III), and 1995–2023 (DSAS IV). The first three intervals exhibit the same rate (0.14 m/year) but with minor differences in the magnitude of uncertainty (+/− 0.02, +/− 0.01, and +/− 0.01, respectively). In contrast, the average retreat rate for the period 1995–2023 (0.16 +/− 0.03 m yr^{-1}) is considerably higher, potentially reflecting greater statistical uncertainty due to the shorter duration and limited scale of this dataset (see Section 5). Our estimates also indicate that, for each interval investigated, the cliff's distal margins experience consistently higher retreat rates than the mid sections (Figure 10); the highest rate of retreat (0.39 m yr^{-1}) occurred in the westernmost part of the cliff between 1995 and 2023.

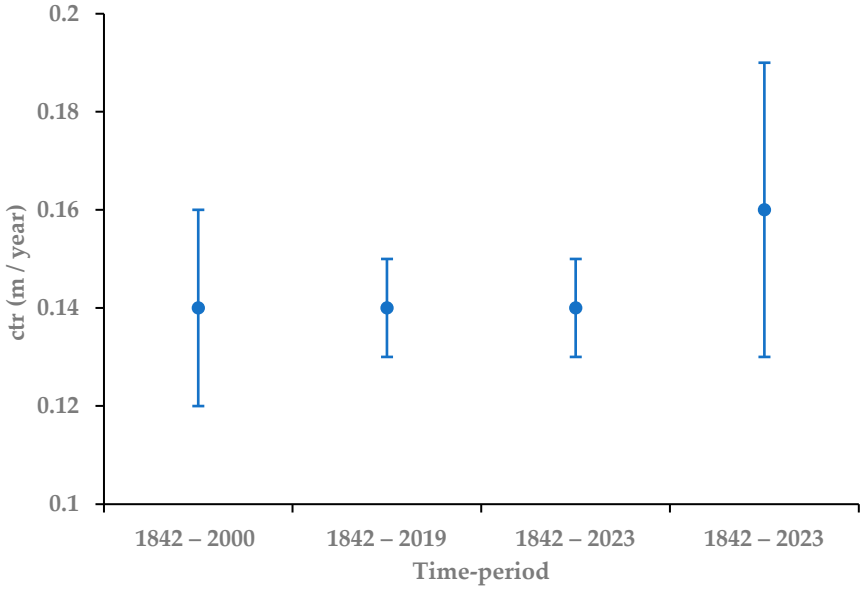

Figure 9. Average cliff top retreat rates for the periods 1842–2000 (DSAS I), 1842–2019 (DSAS II), 1842–2023 (DSAS III), and 1995–2023 (DSAS IV).

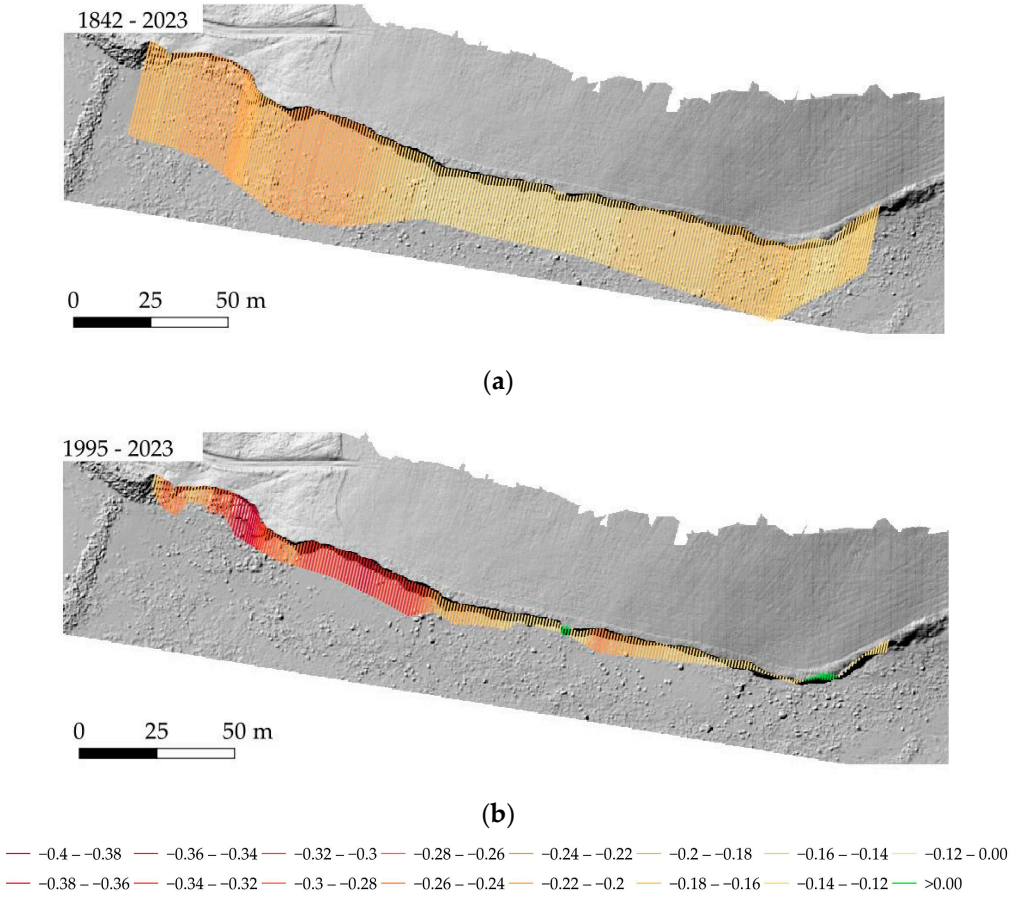

Figure 10. Spatial distribution of cliff top retreat rates for (**a**) 1842–2023 (DSAS III) and (**b**) 1995–2023 (DSAS IV).

4.3. Storm Conditions

Applying our storm-detection criteria to 26 months of offshore hydrodynamic data, we detected a total of 30 storms between January 2018 and February 2020. As anticipated, both Hs and storm duration varied seasonally, being greatest during the winter months (December, January, and February). Wave direction was seasonally constant (322–325°; toward east-southeast), reflecting the influence of coastline configuration (Figure 11 and Table 6). Together, the maximum significant wave heights and storm durations illustrate the exposure of the Knocknagoneen cliff to high-energy storm events.

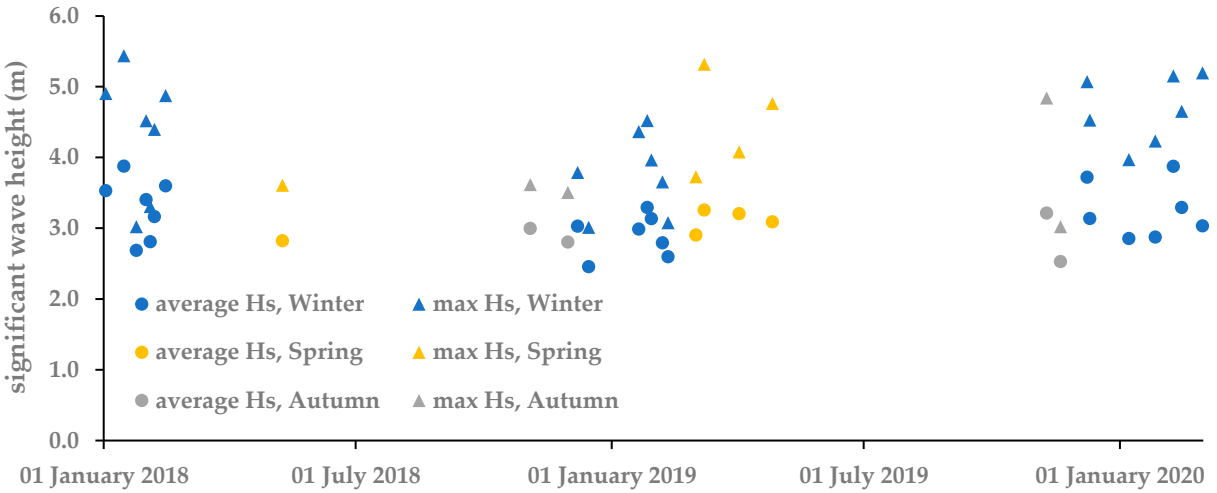

Figure 11. The average and maximum significant wave height (H_s) during storm events in inner Galway Bay between 1 January 2018 and 29 February 2020.

Table 6. Storm events between 1 January 2018 and 29 February 2020, based on detected averaged and max significant wave height (Hs).

	# Storms	Hs Average (m)	Hs Max (m)	Direction °	Duration Average (hrs)
Winter	21	3.15	5.44	322	95
Spring	5	3.06	5.32	323	62
Summer	0				
Autumn	4	2.89	4.84	325	61

5. Discussion

As reported by previous studies [18,76], estimates of cliff retreat rate can differ markedly depending on the method used. Our short- (28 years) and long-term (181 years) DSAS-based estimates for cliff top retreat (0.14–0.16 m yr^{-1}) are double the cliff face retreat rates predicted by the short-term (4.4 years) PC analysis (0.077 m yr^{-1}), a discrepancy with clear implications for the viability of long-term predictions of coastal change. [18] proposed two plausible causes for this offset, the first being that calculated differences in retreat rates signify variability in the magnitude and frequency of erosional events. Whereas cliff top retreat is driven by larger yet more periodic events (e.g., driven by undermining), cliff face retreat reflects the impact of lower-magnitude, higher-frequency events [16,18,77]. Secondly, [18] suggested that disparate estimates arise because the methods themselves are different: cliff top change is calculated directly from differences in cliff top position, whereas cliff face changes are calculated via the horizontal displacement of an area [18]. Moreover, at our site, average rates of cliff top retreat might be biased by the relatively high rates observed at the cliff's western end (as much as 0.2 m/year), which are almost double those in the middle part (0.1 m/year).

As depicted in Figure 1, the Knocknagoneen cliff face is fronted by a shore platform extending as much as 235 m into Galway Bay, which provides clear geologic evidence for the drumlin's former areal extent. According to our two estimates of cliff retreat, this platform began forming either as early as 1700 years ago (PC analysis) or as late as 1500 years ago (DSAS analysis), with the important caveats that cliff erosion may not have been linear nor sea level static during this time. For instance, current estimates of marine inundation in Galway Bay remain variable, suggesting that sea level rose to within the modern intertidal zone during the middle Holocene [57], several millennia later at ~3 ka [78], or as recent as 1500–1000 years ago [58]. We note that should the modern retreat rate for Knocknagoneen be representative of the longer term, it would align broadly with the model of a more recent marine incursion in Galway Bay [58].

Incorporating the three-dimensional PC analysis into a GIS affords valuable new insight into the spatial and temporal distribution of cliff changes (area and volume) and the effective measurement of cliff retreat rates. Further, quantification of sediment losses and gains provides information on overall cliff stability and can be correlated with other spatial data such as lithology and geologic structures. In our study, the volume change results are dominated by the removal of the prominent talus slope at the base of the cliff's western section (Figure 12). The erosion of the talus slope also explains the higher erosion and cliff face retreat rates at the western section of the cliff.

Figure 12. Removal of the prominent talus slope between 11 January 2018 and 23 February 2023. For reference, the red arrows mark the same feature (a deformed lens of glaciofluvial material) in both photographs.

Assuming that the Knocknagoneen drumlin has been subject to multiple cycles of talus slope formation and removal over a protracted period (centuries to millennia), our short-term study provides highly detailed measurements of one part of this cycle—talus slope removal—for a single location along the cliff. It is clear from our results that the aperiodic formation of unconsolidated talus at the cliff base actively protects the lower face from wave erosion [7,10,76,79]. Thus, the cliff functions as a cascading system in which sediment removed from the face accumulates at its natural angle of repose within the talus slope before being undercut and steepened by marine forces [10,33]. The destabilised deposit is removed by wave actions and incorporated into the local littoral cell. During these relatively short period cycles, when the talus debris is stored and removed at the cliff foot, Knocknagoneen can be considered a periodically transport-limited (pTL) cliff on the continuum of transportational cliff types described by [33]. For longer periods (decades–centuries), the drumlin can be considered a supply-limited system (SL) as the rapid disposal of the talus slope debris permits continuous wave erosion of the cliff base [33]. Nonetheless, we recognise that any estimates of cliff face and cliff top retreat will vary significantly depending on where within these cycles of talus slope formation–removal the observation period occurs, with important ramifications for the timing of surveys and viability of associated results [33,77,80]. Ultimately, we suggest that the conceptual model of [33,81] is applicable to our study site and propose that, over the course of our repeated surveys, we measured components C–A (Figure 13), during which the talus cone got eroded, and cliff retreat was reinstated and B–C (Figure 13) where there is no protection by the talus cone and marine forces result in erosion of the cliff and increased cliff retreat.

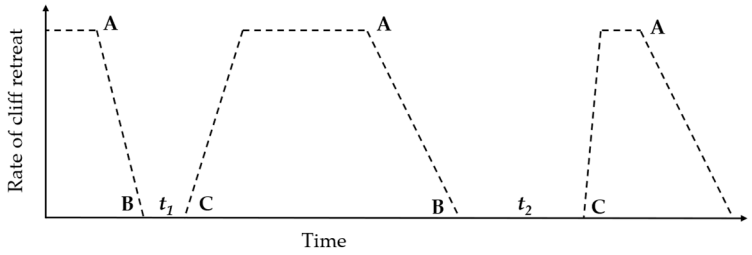

Figure 13. Cliff retreat rates vary over time depending on the formation and erosion of a talus slope at the cliff base (pTL cliff type). Cycles of talus forming and removal are aperiodic; e.g., Time 1 (t_1) ≠ Time 2 (t_2) are time periods when the talus slope exists. Component A–B reflects the gradual growth of the talus slope, which reduces cliff erosion; component B–C represents protection of the cliff base from storm waves by talus; component C–A reflects the gradual removal of talus, resulting in the reactivation of cliff erosion and a decrease in cliff width. Figure adapted from [33].

It is noteworthy that the Knocknagoneen and Knocknacarragh drumlin cliffs have been retreating in a very linear fashion over the past thousands of years, producing very straight cliff lines. The results show that the spatial variability in cliff face retreat was similar for both sections once the talus slope was removed. Perhaps, this feature is not surprising given the homogenous till composition of both landforms. Being only partially consolidated, glaciogenic sediments such as basal diamictons are highly prone to erosion, scarping, and slumping in high-wave-energy environments such as Galway Bay. Together, these geomorphic processes drive the aperiodic development of basal talus slopes that are subsequently washed away during winter storms, while the continuous cycle of sediment delivery to the coastal littoral cell fosters the formation of features such as fringing barriers (Figures 1 and 3). Furthermore, within active marine wetlands (saltmarsh and mudflats) such as Rusheen Bay, immediately north of Knocknagoneen (Figure 1), the deposition of sediment derived from the drumlin face must match or surpass sea level rise if equilibrium is to be maintained within the basin.

Although we attribute coastal cliff erosion to marine erosion mechanisms, we are cognisant of the potential role of subaerial mechanisms acting on the cliff. Based on repeat visits to the site, there was very limited evidence of rainfall-induced erosion processes such as rilling impacting cliff stability. It is noted that rainfall events can influence subsurface pore pressures and cliff stability that are not discernible during site visits [82]. The potential influence of subaerial processes requires further investigation, especially in wet climates like Galway (see Section 2.1), but it is assumed that marine forces are the dominant control on cliff stability.

6. Conclusions

We combined historical data (1842–2000) and contemporary UAV surveys (2019–2023) to measure rates of cliff top and cliff face retreat along a 250 m wide coastal drumlin in Galway Bay. Our reconstructions suggest that the average cliff top retreat rate between 1842 and 2023 (0.14 +/− 0.02 m yr^{-1}) was higher than the rate of cliff face retreat for the period 2019–2023 (0.08 +/− 0.02 m yr^{-1}). In agreement with previous investigations, we found that estimated rates of cliff retreat differ markedly depending on the method used, with the DSAS-based rates being approximately double those predicted by PC analysis. We attribute this discrepancy most likely to differences in methodology, which reiterates that method choice will have important implications for cliff retreat forecasting. Nevertheless, probable differences in cliff top and cliff face erosion processes should also be considered.

The Knocknagoneen escarpment functions as a cascading system in which sediment removed from the cliff face accumulates at its natural angle of repose within the talus slope, which is, in turn, undercut and steepened by wave action. Remobilised sediment is then transported by wave action and incorporated into the local littoral cell. The repeat cycles of talus slope formation and removal in this high wave energy climate suggest that the drumlin transitions between a periodically transport-limited system and supply-

limited system over short- and long-time periods, respectively, on the continuum of cliff types. Although direct precipitation undoubtedly plays some role in cliff face stability, we conclude that this factor is secondary compared to marine mechanisms, which dominate the cascading system at this soft rocky landform.

Author Contributions: Conceptualization, G.M.R., E.J.F. and G.R.M.B.; Formal analysis, G.M.R.; Investigation, G.M.R., E.J.F. and G.R.M.B.; Resources, E.J.F.; Data curation, G.M.R. and E.J.F.; Writing—original draft, G.M.R.; Writing—review & editing, G.M.R., E.J.F. and G.R.M.B.; Visualization, G.M.R. and E.J.F.; Supervision, G.R.M.B. All authors have read and agreed to the published version of the manuscript.

Funding: This research was founded by SFI Research Centre in Applied Geosciences (iCRAG) grant # 13/RC/2029_2.

Data Availability Statement: SfM data are available upon author request. Historical maps and orthophotos can be requested from Ordnance Survey Ireland.

Acknowledgments: We would like to acknowledge the Ordnance Survey Ireland (OSI) for providing free access to maps and orthophotos.

Conflicts of Interest: The authors declare no conflict of interest.

References

1. Knight, J.; Harrison, S. Paraglacial Evolution of the Irish Landscape. *Ir. Geogr.* **2018**, *51*, 171–186. [CrossRef]
2. Hanvey, P.M. The Sedimentology and Genesis of Late-Pleistocene Drumlins in Counties Mayo and Donegal, Western Ireland. Ph.D. Thesis, University of Ulster, Coleraine, UK, 1988.
3. Greenwood, R.O.; Orford, J.D. Temporal Patterns and Processes of Retreat of Drumlin Coastal Cliffs—Strangford Lough, Northern Ireland. *Geomorphology* **2008**, *94*, 153–169. [CrossRef]
4. McCabe, A.M.; Dardis, G.F. Sedimentology and Depositional Setting of Late Pleistocene Drumlins, Galway Bay, Western Ireland. *J. Sediment. Res.* **1989**, *59*, 944–959. [CrossRef]
5. Department of Housing, Local Government and Heritage and the Office of Public Works. *Report of the Inter-Departmental Group on National Coastal Change Management Strategy*; Government of Ireland: Dublin, Ireland, 2023; p. 108.
6. Emery, K.O.; Kuhn, G.G. Sea Cliffs: Their Processes, Profiles, and Classification. *Geol. Soc. Am. Bull.* **1982**, *93*, 644. [CrossRef]
7. Prémaillon, M.; Regard, V.; Dewez, T.J.B.; Auda, Y. GlobR2C2 (Global Recession Rates of Coastal Cliffs): A Global Relational Database to Investigate Coastal Rocky Cliff Erosion Rate Variations. *Earth Surf. Dyn.* **2018**, *6*, 651–668. [CrossRef]
8. Young, A.P.; Carilli, J.E. Global Distribution of Coastal Cliffs. *Earth Surf. Process. Landf.* **2019**, *44*, 1309–1316. [CrossRef]
9. Cullen, N. A Study of Rock Coast Erosion on the Atlantic Coast of Ireland. Ph.D. Thesis, Trinity College Dublin, School of Natural Sciences, Dublin, Ireland, 2019.
10. Caplain, B.; Astruc, D.; Regard, V.; Moulin, F.Y. Cliff Retreat and Sea Bed Morphology under Monochromatic Wave Forcing: Experimental Study. *Comptes Rendus Geosci.* **2011**, *343*, 471–477. [CrossRef]
11. Westoby, M.J.; Brasington, J.; Glasser, N.F.; Hambrey, M.J.; Reynolds, J.M. 'Structure-from-Motion' Photogrammetry: A Low-Cost, Effective Tool for Geoscience Applications. *Geomorphology* **2012**, *179*, 300–314. [CrossRef]
12. Gonçalves, J.A.; Henriques, R. UAV Photogrammetry for Topographic Monitoring of Coastal Areas. *J. Photogramm. Remote Sens.* **2015**, *104*, 101–111. [CrossRef]
13. Luetzenburg, G.; Townsend, D.; Svennevig, K.; Bendixen, M.; Bjørk, A.A.; Eidam, E.F.; Kroon, A. Sedimentary Coastal Cliff Erosion in Greenland. *J. Geophys. Res. Earth Surf.* **2023**, *128*, e2022JF007026. [CrossRef]
14. Ruggiero, P.; Kratzmann, M.G.; Himmelstoss, E.A.; Reid, D.; Allan, J.; Kaminsky, G. *National Assessment of Shoreline Change: Historical Shoreline Change along the Pacific Northwest Coast*; Open-File Report; United States Geological Survey: Reston, VA, USA, 2013.
15. Irrgang, A.M.; Lantuit, H.; Manson, G.K.; Günther, F.; Grosse, G.; Overduin, P.P. Variability in Rates of Coastal Change along the Yukon Coast, 1951 to 2015. *J. Geophys. Res. Earth Surf.* **2018**, *123*, 779–800. [CrossRef]
16. Rosser, N.J.; Brain, M.J.; Petley, D.N.; Lim, M.; Norman, E.C. Coastline Retreat via Progressive Failure of Rocky Coastal Cliffs. *Geology* **2013**, *41*, 939–942. [CrossRef]
17. Williams, J.G.; Rosser, N.J.; Hardy, R.J.; Brain, M.J.; Afana, A.A. Optimising 4-D Surface Change Detection: An Approach for Capturing Rockfall Magnitude–Frequency. *Earth Surf. Dyn.* **2018**, *6*, 101–119. [CrossRef]
18. Swirad, Z.M.; Young, A.P. Spatial and Temporal Trends in California Coastal Cliff Retreat. *Geomorphology* **2022**, *412*, 108318. [CrossRef]
19. Swirad, Z.M.; Rosser, N.J.; Brain, M.J. Identifying Mechanisms of Shore Platform Erosion Using Structure-from-Motion (SfM) Photogrammetry. *Earth Surf. Process. Landf.* **2019**, *44*, 1542–1558. [CrossRef]

20. Vanneschi, C.; Camillo, M.; Aiello, E.; Bonciani, F.; Salvini, R. SfM-MVS Photogrammetry for Rockfall Analysis and Hazard Assessment along the Ancient Roman via Flaminia Road at the Furlo Gorge (Italy). *ISPRS Int. J. Geo-Inf.* **2019**, *8*, 325. [CrossRef]
21. Piermattei, L.; Carturan, L.; Guarnieri, A. Use of Terrestrial Photogrammetry Based on Structure-from-Motion for Mass Balance Estimation of a Small Glacier in the Italian Alps: SfM-MVS approach for glacier mass balance estimation. *Earth Surf. Process. Landf.* **2015**, *40*, 1791–1802. [CrossRef]
22. Marcer, M.; Stentoft, P.A.; Bjerre, E.; Cimoli, E.; Bjørk, A.; Stenseng, L.; Machguth, H. Three Decades of Volume Change of a Small Greenlandic Glacier Using Ground Penetrating Radar, Structure from Motion, and Aerial Photogrammetry. *Arct. Antarct. Alp. Res.* **2017**, *49*, 411–425. [CrossRef]
23. Colomina, I.; Molina, P. Unmanned Aerial Systems for Photogrammetry and Remote Sensing: A Review. *ISPRS J. Photogramm. Remote Sens.* **2014**, *92*, 79–97. [CrossRef]
24. James, M.R.; Robson, S.; d'Oleire-Oltmanns, S.; Niethammer, U. Optimising UAV Topographic Surveys Processed with Structure-from-Motion: Ground Control Quality, Quantity and Bundle Adjustment. *Geomorphology* **2017**, *280*, 51–66. [CrossRef]
25. James, L.A.; Hodgson, M.E.; Ghoshal, S.; Latiolais, M.M. Geomorphic Change Detection Using Historic Maps and DEM Differencing: The Temporal Dimension of Geospatial Analysis. *Geomorphology* **2012**, *137*, 181–198. [CrossRef]
26. DaSilva, M.; Miot Da Silva, G.; Hesp, P.A.; Bruce, D.; Keane, R.; Moore, C. Assessing Shoreline Change Using Historical Aerial and RapidEye Satellite Imagery (Cape Jaffa, South Australia). *J. Coast. Res.* **2021**, *37*, 468–483. [CrossRef]
27. Hapke, C.J.; Reid, D. *National Assessment of Shoreline Change, Part 4: Historical Coastal Cliff Retreat along the California Coast*; United States Geological Survey: Reston, VA, USA, 2007.
28. Kenny, P. *MapGenie*; Ordnance Survey Ireland: Dublin, Ireland, 2023.
29. Boardman, J.; Favis-Mortlock, D.T. The Use of Erosion Pins in Geomorphology. In *Geomorphological Techniques (Online Edition)*; Chapter, 3.5.3; Cook, S.J., Clarke, L.E., Nield, J.M., Eds.; British Society for Geomorphology: London, UK, 2016; ISSN 2047-0371. ISBN 2047-0371.
30. Jaud, M.; Le Dantec, N.; Parker, K.; Lemon, K.; Lendre, S.; Delacourt, C.; Gomes, R.C. How to Include Crowd-Sourced Photogrammetry in a Geohazard Observatory—Case Study of the Giant's Causeway Coastal Cliffs. *Remote Sens.* **2022**, *14*, 3243. [CrossRef]
31. Wernette, P.; Miller, I.M.; Ritchie, A.W.; Warrick, J.A. Crowd-Sourced SfM: Best Practices for High Resolution Monitoring of Coastal Cliffs and Bluffs. *Cont. Shelf Res.* **2022**, *245*, 104799. [CrossRef]
32. Young, A.P. Decadal-Scale Coastal Cliff Retreat in Southern and Central California. *Geomorphology* **2018**, *300*, 164–175. [CrossRef]
33. Sunamura, T. Rocky Coast Processes: With Special Reference to the Recession of Soft Rock Cliffs. *Procirca Jpn. Acad. Ser. B* **2015**, *91*, 481–500. [CrossRef] [PubMed]
34. Gómez-Pazo, A.; Pérez-Alberti, A.; Trenhaile, A. Tracking the Behavior of Rocky Coastal Cliffs in Northwestern Spain. *Environ. Earth Sci.* **2021**, *80*, 757. [CrossRef]
35. Utting, D.; Gallacher, A. *Coastal Environments and Erosion in Southwest St. Georges Bay, Antigonish County*; Report ME 2009-1; Nova Scotia Department of Natural: Halifax, NS, Canada, 2008.
36. Nunes, M.; Ferreira, Ó.; Loureiro, C.; Baily, B. Beach and Cliff Retreat Induced by Storm Groups at Forte Novo, Algarve (Portugal). *J. Coast. Res.* **2011**, *64*, 795–799.
37. McKenna, J.; Carter, R.W.G.; Bartlett, D. Coast Erosion in Northeast Ireland: Part II Cliffs and Shore Platforms. *Ir. Geogr.* **1992**, *25*, 111–128. [CrossRef]
38. Thébaudeau, B.; Trenhaile, A.S.; Edwards, R.J. Modelling the Development of Rocky Shoreline Profiles along the Northern Coast of Ireland. *Geomorphology* **2013**, *203*, 66–78. [CrossRef]
39. Cullen, N.D.; Bourke, M.C. Clast Abrasion of a Rock Shore Platform on the Atlantic Coast of Ireland: Clast Abrasion of a Rock Shore Platform. *Earth Surf. Process. Landf.* **2018**, *43*, 2627–2641. [CrossRef]
40. Benjamin, J. Regional-Scale Controls on Rockfall Occurrence. Ph.D. Thesis, Durham University, Durham, UK, 2018.
41. Shadrick, J.R.; Hurst, M.D.; Piggott, M.D.; Hebditch, B.G.; Seal, A.J.; Wilcken, K.M.; Rood, D.H. Multi-Objective Optimisation of a Rock Coast Evolution Model with Cosmogenic ^{10}Be Analysis for the Quantification of Long-Term Cliff Retreat Rates. *Earth Surf. Dyn.* **2021**, *9*, 1505–1529. [CrossRef]
42. Shadrick, J.R.; Rood, D.H.; Hurst, M.D.; Piggott, M.D.; Wilcken, K.M.; Seal, A.J. Constraints on Long-Term Cliff Retreat and Intertidal Weathering at Weak Rock Coasts Using Cosmogenic ^{10} Be, Nearshore Topography and Numerical Modelling. *Earth Surf. Dyn.* **2023**, *11*, 429–450. [CrossRef]
43. Dornbusch, U.; Robinson, D.A.; Moses, C.A.; Williams, R.B.G. Temporal and Spatial Variations of Chalk Cliff Retreat in East Sussex, 1873 to 2001. *Mar. Geol.* **2008**, *249*, 271–282. [CrossRef]
44. Smith, R. Implications of Proposed Engineering for Soft Rock Coast & Saltmarsh Sediment Dynamics. Master's Thesis, University of Galway, Galway, Ireland, 2019.
45. Hennessy, R.; Meehan, R.; Gallagher, V.; Parkes, M.; Glanville, C. *The Geological Heritage of Galway City. An Audit of County Geological Sites in Galway City*; Geological Survey Ireland: Dublin, Ireland, 2020.
46. Peel, M.C.; Finlayson, B.L.; McMahon, T.A. Updated World Map of the Köppen-Geiger Climate Classification. *Hydrol. Earth Syst. Sci.* **2007**, *11*, 1633–1644. [CrossRef]
47. Fiaschi, S.; Holohan, E.; Sheehy, M.; Floris, M. PS-InSAR Analysis of Sentinel-1 Data for Detecting Ground Motion in Temperate Oceanic Climate Zones: A Case Study in the Republic of Ireland. *Remote Sens.* **2019**, *11*, 348. [CrossRef]

48. Ren, L.; Nash, S.; Hartnett, M. Observation and Modeling of Tide- and Wind-Induced Surface Currents in Galway Bay. *Water Sci. Eng.* **2015**, *8*, 345–352. [CrossRef]
49. Calvino, C.; Dabrowski, T.; Dias, F. A Study of the Sea Level and Current Effects on the Sea State in Galway Bay, Using the Numerical Model COAWST. *Ocean. Dyn.* **2022**, *72*, 761–774. [CrossRef]
50. Calvino, C.; Dabrowski, T.; Dias, F. A Study of the Wave Effects on the Current Circulation in Galway Bay, Using the Numerical Model COAWST. *Coast. Eng.* **2023**, *180*, 104251. [CrossRef]
51. Atan, R.; Goggins, J.; Harnett, M.; Agostinho, P.; Nash, S. Assessment of Wave Characteristics and Resource Variability at a 1/4-Scale Wave Energy Test Site in Galway Bay Using Waverider and High Frequency Radar (CODAR) Data. *Ocean. Eng.* **2016**, *117*, 272–291. [CrossRef]
52. Miccadei, E.; Mascioli, F.; Ricci, F.; Piacentini, T. Geomorphology of Soft Clastic Rock Coasts in the Mid-Western Adriatic Sea (Abruzzo, Italy). *Geomorphology* **2019**, *324*, 72–94. [CrossRef]
53. ESRI Esri Gray (Light) 2021. WMS Server. Available online: https://services.arcgisonline.com/ArcGIS/rest/services/Canvas/World_Light_Gray_Base/MapServer/tile/{z}/{y}/{x} (accessed on 26 January 2024).
54. Google Google Satellite 2024. WMS Server. Available online: https://mt1.google.com/vt/lyrs=s&x={x}&y={y}&z={z} (accessed on 26 January 2024).
55. Greenwood, S.L.; Clark, C.D. Reconstructing the Last Irish Ice Sheet 1: Changing Flow Geometries and Ice Flow Dynamics Deciphered from the Glacial Landform Record. *Quat. Sci. Rev.* **2009**, *28*, 3085–3100. [CrossRef]
56. Smith, M.J.; Knight, J. Palaeoglaciology of the Last Irish Ice Sheet Reconstructed from Striae Evidence. *Quat. Sci. Rev.* **2011**, *30*, 147–160. [CrossRef]
57. Clark, C.D.; Hughes, A.L.C.; Greenwood, S.L.; Spagnolo, M.; Ng, F.S.L. Size and Shape Characteristics of Drumlins, Derived from a Large Sample, and Associated Scaling Laws. *Quat. Sci. Rev.* **2009**, *28*, 677–692. [CrossRef]
58. Spagnolo, M.; Clark, C.D.; Hughes, A.L.C.; Dunlop, P.; Stokes, C.R. The Planar Shape of Drumlins. *Sediment. Geol.* **2010**, *232*, 119–129. [CrossRef]
59. Foreman, A.C.; Bromley, G.R.M.; Hall, B.L.; Jackson, M.S. A 10Be-Dated Record of Glacial Retreat in Connemara, Ireland, Following the Last Glacial Maximum and Implications for Regional Climate. *Palaeogeogr. Palaeoclimatol. Palaeoecol.* **2022**, *592*, 110901. [CrossRef]
60. Williams, D.M.; Doyle, E. Dates from Drowned Mid-Holocene Landscapes on the Central Western Irish Seaboard. *Ir. J. Earth Sci.* **2014**, *32*, 23–27. [CrossRef]
61. O'Connell, M.; Molloy, K. Mid- and Late-Holocene Environmental Change in Western Ireland: New Evidence from Coastal Peats and Fossil Timbers with Particular Reference to Relative Sea-Level Change. *Holocene* **2017**, *27*, 1825–1845. [CrossRef]
62. Schettler, G.; Romer, R.L.; O'Connell, M.; Molloy, K. Holocene Climatic Variations and Postglacial Sea-Level Rise Geochemically Recorded in the Sediments of the Brackish Karst Lake an Loch Mor, Western Ireland. *Boreas* **2006**, *35*, 674–693. [CrossRef]
63. Himmelstoss, E.A.; Farris, A.S.; Henderson, R.E.; Kratzmann, M.G.; Ergul, A.; Zhang, O.; Zichichi, J.L.; Thieler, E.R. *Digital Shoreline Analysis System*; Version 5; U.S. Geological Survey: Reston, VA, USA, 2018.
64. Himmelstoss, E.A.; Henderson, R.E.; Kratzmann, M.G.; Farris, A.S. *Digital Shoreline Analysis System (DSAS) Version 5.1 User Guide*; Open-File Report; U.S. Geological Survey: Reston, VA, USA, 2021.
65. Lague, D.; Brodu, N.; Leroux, J. Accurate 3D Comparison of Complex Topography with Terrestrial Laser Scanner: Application to the Rangitikei Canyon (N-Z). *ISPRS J. Photogramm. Remote Sens.* **2013**, *82*, 10–26. [CrossRef]
66. CloudCompare CloudCompare 2022. Available online: https://www.cloudcompare.org/release/notes/20220330/ (accessed on 3 July 2023).
67. Agisoft LCC. *Agisoft Metashape User Manual Professional Edition*; Version 2.0; Agisoft LLC: Saint Petersburg, Russia, 2023.
68. Cullen, N.D.; Verma, A.K.; Bourke, M.C. A Comparison of Structure from Motion Photogrammetry and the Traversing Micro-Erosion Meter for Measuring Erosion on Shore Platforms. *Earth Surf. Dyn.* **2018**, *6*, 1023–1039. [CrossRef]
69. Kromer, R.; Lato, M.; Hutchinson, D.J.; Gauthier, D.; Edwards, T. Managing Rockfall Risk through Baseline Monitoring of Precursors Using a Terrestrial Laser Scanner. *Can. Geotech. J.* **2017**, *54*, 953–967. [CrossRef]
70. Chen, Y.; Medioni, G. Object Modeling by Registration of Multiple Range Images. In Proceedings of the 1991 IEEE International Conference on Robotics and Automation, Sacramento, CA, USA, 9–11 April 1991; pp. 2724–2729.
71. Hartmeyer, I.; Keuschnig, M.; Delleske, R.; Krautblatter, M.; Lang, A.; Schrott, L.; Prasicek, G.; Otto, J.-C. A 6-Year Lidar Survey Reveals Enhanced Rockwall Retreat and Modified Rockfall Magnitudes/Frequencies in Deglaciating Cirques. *Earth Surf. Dyn.* **2020**, *8*, 753–768. [CrossRef]
72. OSI MapGenie WMS 2023. WMTS Server. Available online: https://ogcmapgenie.osi.ie/data/rest/services/ITM (accessed on 3 July 2023).
73. Asoni, S.G.; Stavrou, A.; Lawrence, J.A. Developing a GIS Based Methodology for Coastal Chalk Cliff Retreat Using Multiple Datasets. In Proceedings of the Engineering in Chalk, London, UK, 17–18 January 2018; pp. 369–374.
74. Terres De Lima, L.; Fernández-Fernández, S.; Marcel De Almeida Espinoza, J.; Da Guia Albuquerque, M.; Bernardes, C. End Point Rate Tool for QGIS (EPR4Q): Validation Using DSAS and AMBUR. *ISPRS Int. J. Geo-Inf.* **2021**, *10*, 162. [CrossRef]
75. Vallarino Castillo, R.; Negro Valdecantos, V.; Moreno Blasco, L. Shoreline Change Analysis Using Historical Multispectral Landsat Images of the Pacific Coast of Panama. *J. Mar. Sci. Eng.* **2022**, *10*, 1801. [CrossRef]

76. Genz, A.S.; Fletcher, C.H.; Dunn, R.A.; Frazer, L.N.; Rooney, J.J. The Predictive Accuracy of Shoreline Change Rate Methods and Alongshore Beach Variation on Maui, Hawaii. *J. Coast. Res.* **2007**, *23*, 87–105. [CrossRef]
77. Guisado-Pintado, E.; Jackson, D.W.T. Coastal Impact from High-Energy Events and the Importance of Concurrent Forcing Parameters: The Cases of Storm Ophelia (2017) and Storm Hector (2018) in NW Ireland. *Front. Earth Sci.* **2019**, *7*, 190. [CrossRef]
78. Zelinsky, D.A. *Tropical Cyclone Report: Hurricane Lorenzo (AL132019)*; United States National Hurricane Center: Miami, FL, USA, 2019.
79. Lim, M.; Rosser, N.J.; Allison, R.J.; Petley, D.N. Erosional Processes in the Hard Rock Coastal Cliffs at Staithes, North Yorkshire. *Geomorphology* **2010**, *114*, 12–21. [CrossRef]
80. Jordan, S.F.; Murphy, B.T.; O'Reilly, S.S.; Doyle, K.P.; Williams, M.D.; Grey, A.; Lee, S.; McCaul, M.V.; Kelleher, B.P. Mid-Holocene Climate Change and Landscape Formation in Ireland: Evidence from a Geochemical Investigation of a Coastal Peat Bog. *Org. Geochem.* **2017**, *109*, 67–76. [CrossRef]
81. Williams, J.G.; Rosser, N.J.; Hardy, R.J.; Brain, M.J. The Importance of Monitoring Interval for Rockfall Magnitude-Frequency Estimation. *J. Geophys. Res. Earth Surf.* **2019**, *124*, 2841–2853. [CrossRef]
82. Brooks, S.M.; Spencer, T.; Boreham, S. Deriving Mechanisms and Thresholds for Cliff Retreat in Soft-Rock Cliffs under Changing Climates: Rapidly Retreating Cliffs of the Suffolk Coast, UK. *Geomorphology* **2012**, *153–154*, 48–60. [CrossRef]